Exp Fluids (2009) 46:527–537
DOI 10.1007/s00348-008-0578-1

RESEARCH ARTICLE

A note on wind-tunnel turbulence measurements with DPIV

G. R. Spedding · A. Hedenström · L. C. Johansson

Received: 23 January 2008 / Revised: 3 October 2008 / Accepted: 7 October 2008 / Published online: 26 October 2008

Abstract At moderate Reynolds numbers ($10^4 \leq Re \leq 10^5$), the performance of lifting surfaces is strongly affected by the potential for laminar boundary layer separation and subsequent reattachment and the use of high-quality, low-turbulence wind tunnels is essential in characterising flight at comparatively small scales (where the wing chord may be from 1 to 5 cm in length) and low speeds (on the order of 10 m/s). Measurement of the existing turbulence levels in such facilities is hard and has not been achieved using DPIV methods due to the relatively small bandwidth of measurable velocities. A series of experiments is reported here where DPIV sampling parameters are driven beyond their normal range in an attempt to measure turbulence levels in a low turbulence wind tunnel. The results show that DPIV can measure the background turbulence, and therefore its instantaneous structure. The measurements also reveal certain challenges in investigating the aerodynamic performance of small-scale flying devices.

G. R. Spedding
Department of Aerospace and Mechanical Engineering,
University of Southern California,
Los Angeles, CA 90089, USA

Present Address:
G. R. Spedding (✉)
Department of Mechanical and Aeronautical Engineering,
University of Pretoria, Pretoria 0002, South Africa
e-mail: geoff.spedding@up.ac.za

A. Hedenström · L. C. Johansson
Department of Theoretical Ecology,
Lund University, Lund, Sweden
e-mail: anders.hedenstrom@teorekol.lu.se

L. C. Johansson
e-mail: christoffer.johansson@teorekol.lu.se

1 Introduction

The purpose of a wind tunnel is to generate a uniform, steady mean flow, U, over a small part of it, known as the test section. Ideally, the flow should not vary in any of the spatial directions $\{x, y, z\}$ (streamwise, spanwise, and vertical) and should not vary with time. Wind tunnels are constructed so that departures from this ideal are small. The departures that do exist are commonly termed *turbulence*, though they are not simply related to the usual fluid mechanical definition of turbulence (Tennekes and Lumley 1972). Small, or even moderate levels of turbulence (we will retain the traditional wind tunnel usage of this term for the moment) need not be detrimental; one can argue that the higher the turbulence, the higher the effective Reynolds number of the wind tunnel flow (see Barlow et al. 1999, p. 227). However, this connection is not very straight-forward, even if the so-called turbulence characteristics do model the full-scale application correctly.

Because wind tunnels are engineered to produce very small variations about the steady mean U, it is hard to measure the remaining fluctuations that do exist. Two methods are in common use. The first uses the known sharp reduction in drag around a sphere at some transition Reynolds number (see Barlow et al. 1999). This transition Reynolds number is a function of ambient turbulence, and so a wind tunnel can be characterised by a turbulence factor,

$$\mathrm{TF} = \frac{385000}{R_{\mathrm{obs}}}, \tag{1}$$

where R_{obs} is the observed transition Reynolds number, and the number 385000 is the Reynolds number at which transition occurs in turbulence-free conditions (as measured from atmospheric flight tests). More precise measurement of turbulence properties can be accomplished using hot-wire

anemometry. Operated in strong overheat, the hot-wire set-up can be tuned for maximum sensitivity to fluctuations about the mean at any given speed, and this kind of method is used for more serious descriptions. Dryden et al. (1937) and Dryden and Kuethe (1929) remain standard references for wind tunnel turbulence measurements, where hot-wire and turbulence sphere measurements are compared. Hot-wire rakes and traverse systems allow maps of average fluctuating velocity components to be measured. Nevertheless, it is still common practice to characterise a wind tunnel with one single number,

$$\text{percent turbulence} = \frac{q}{U} \times 100, \tag{2}$$

where q is either the root mean square of the fluctuating streamwise velocity component, $u - U$, or the rms of all measurable fluctuating components in

$$q = \left((u-U)^2 + v^2 + w^2\right)^{\frac{1}{2}}, \tag{3}$$

averaged over some time interval and over some spatial region.

The significance of the magnitude of the fluctuations, q, depends on the characteristics of the flow. If the length and time scales of interest in the test system differ greatly from those of the remaining disturbances in the tunnel then the latter might be unimportant. One flow configuration that is notoriously sensitive to residual fluctuations is where initially laminar boundary layers approach conditions for separation. This condition is found in low-speed airfoils, whose performance is exquisitely sensitive to details of separation and possible reattachment (Lissaman 1983). In the Reynolds number range $Re_c \equiv Uc/\nu = [10^4–10^5]$, where c is a streamwise chord length and ν is the kinematic viscosity, variations in measured drag can be a factor of 2 different in different facilities (see Lyon et al. 1998, p. 222, for examples). These differences are usually attributed to different behaviour of separation bubbles due to different ambient turbulence characteristics. In any study of airfoils or wings over this range of Re, a correct description of the wind tunnel fluctuations is clearly necessary. Nevertheless, the descriptions that are given rarely stray beyond the single number specification in Eq. 2 (cf. Selig and McGranahan 2004).

Digital Particle Image Velocimetry (DPIV) methods are ubiquitous in experimental fluid mechanics, but cannot easily be used to measure wind tunnel turbulence because the measurement bandwidth is so low. If the largest mean particle image displacement on the sensor is 5 pixels, and the smallest resolvable displacement is 1/20 pixel, then the bandwidth is 100. Fluctuating velocity magnitudes in high-quality wind tunnels are very low, relative to the mean speed, with $q/U \leq 0.05\%$, which is 20 times smaller than the smallest resolvable DPIV measurement under standard operating procedures. Even with some care, reasonable turbulence measurements are elusive, and Spedding et al. (2003a) reported how a systematic decrease in observed turbulence level with increasing DPIV delay time, δt, showed that no reliable turbulence measurement could be reached. Note that the measurement of the residual, low-level turbulence in a clean wind tunnel facility poses a slightly different set of problems than commonly addressed in application of PIV to larger amplitude turbulence problems (e.g. Fincham and Spedding 1997; Adrian et al. 2000; Scarano 2003; Agrawal 2005; Adeyinka and Naterer 2007; Tanaka and Eaton 2007; Lavoie et al. 2007), although the common denominator remains the low bandwidth of PIV methods. The comparatively low velocity bandwidth (compared with a hot-wire, for example, or with a numerical simulation) is a shared characteristic of all PIV algorithms and so the results from this paper are also quite general.

This paper reports on results of an investigation into the feasibility of making wind tunnel turbulence measurements with DPIV methods. It uses an analogue of the hot-wire overheat principle by using very large values of δt that are compensated for by measuring only fluctuating displacements and not mean quantities. This is possible because the flow is otherwise extremely uniform. The instantaneous spatial structure of wind tunnel turbulence can be shown, and some important operating principles of wind tunnels in nominally low-turbulence regimes are found.

2 Materials and methods

2.1 A low-turbulence wind tunnel for bird flight

The wind tunnel used at Lund (Fig. 1) is a standard, closed-circuit, recirculating configuration, with two special modifications that make it especially valuable for research on bird flight. The entire tunnel can be tilted at any angle from $+8°$ (nose down in the test section) to $-6°$, allowing experiments on climbing or descending flight, and most important, on steady gliding flight. The tunnel also has an open section just aft of the test section. This makes it very practical for inserting and removing live animals (or fixed models), and it also removes streamwise pressure gradients there since the flow is open to atmospheric pressure. One further property makes it well-suited for bird/bat flight studies, which is the low turbulence level over most of the test section. The tunnel turbulence properties were carefully measured by single and x-wire hot wire anemometry and streamwise and cross-stream plane maps were made of the magnitude of the average fluctuating velocity. These properties are documented in Pennycuick et al. (1997). The average turbulence levels, q/U, were approximately 0.035%, which is a satisfactorily low number, so

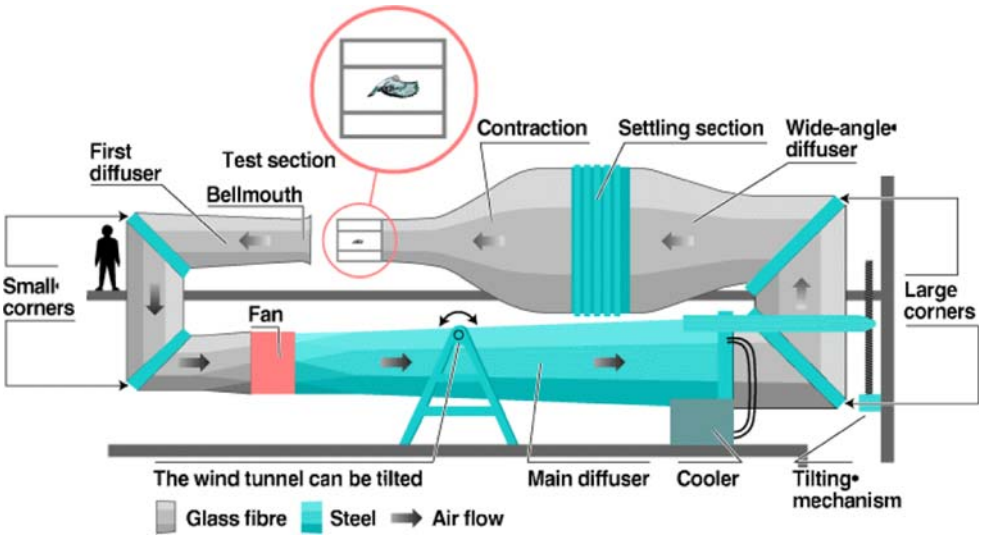

Fig. 1 The wind tunnel configuration includes a pivot about which the wind tunnel can rotate, and an open test section where objects such as live birds can easily be inserted and removed

that results from the tunnel can be reliable and compared with other top quality research wind tunnels. Recall that this is particularly important for $10^4 \leq Re_c \leq 10^5$, which is exactly the range in which small birds and bats operate.

Extensive studies have been made on live, trained (but otherwise unrestrained) birds and bats in this tunnel (e.g. Pennycuick et al. 2000; Park et al. 2001; Rosén and Hedenström 2001; Spedding et al. 2003b; Hedenström et al. 2006; Muijres et al. 2008; Hedenström and Spedding 2008; Henningsson et al. 2008), the latter publications using custom DPIV methods on a two-camera (or equivalent) system that removed the mean flow and allowed the DPIV bandwidth to be concentrated on disturbance quantities. In spite of this, turbulence measurements were not successful when DPIV exposures were set close to appropriate settings for the bird wake studies. Although the wake disturbances could be shown to be significantly above measurement noise, the background turbulence was not.

2.2 Experimental procedure

The flow was seeded by a commercial fog generator (JEM ZR12-AL) placed inside the first diffuser, about 1 m downstream of the bellmouth and covered by a fairing to deflect the flow smoothly. The ability of an individual smoke particle with diameter, $d \approx 1$ μm, and density, ρ, to follow a flow with characteristic length and velocity scales of L and U can be expressed through the Stokes number,

$$St = \frac{\rho d^2 U C_c}{18 \mu L},$$

where μ is the fluid viscosity, and C_c is a slip correction factor (Hinds 1999) that has a value close to one for such particle diameters. If $St \ll 1$, then particle inertia is small relative to variations in the flow streamlines. For $U = 10$ m/s and $L = 2$ cm (as suggested by results to appear in the following sections), then $St \approx 2 \times 10^{-3}$, and so the criterion is satisfied and the smoke particles can be assumed to follow the air flow.

The wind tunnel was run for at least one hour before any experiment (to remove both temperature and velocity fluctuations) and then filled with smoke over a period of about 30 min. During experiments, 20–30 s bursts of smoke were introduced at regular intervals to maintain the particle density (most particularly particles that generate large, bright images; such particles easily meet the 1.5 pixel minimum diameter required for a reasonable sub-pixel estimator to work.). The times between these smoke refills and each experiment were kept constant. The particles were illuminated by pulses from a dual-head Nd:YAG laser (Spectra-Physics PIVII) and imaged onto a Redlake Megaplus II ES4020 12-bit CCD sensor ($2{,}048^2$ pixels) with Nikkor 50 mm f1.4–16 lens. Streams of image pairs were saved directly on a SCSI RAID disk array through an IO Industries DVR Express CL160 interface, controlled by Video Savant software from the same company. Image sequences were saved uncompressed, and analysed using the Correlation Imaging Velocimetry (CIV) algorithms described in Fincham and Spedding (1997) and Fincham and Delerce (2000). Correlation boxes were typically 30 pixels on a side, corresponding to 5 mm in the flow. This is comparable to the laser sheet thickness of 3–4 mm. In the CIV algorithms the correlation box size is unrelated to the search domain size, which is modified by adding a large pre-computed shift as described in the following section.

2.3 Measuring low turbulence levels with DPIV

The basic idea of the original shifted 2-camera system is the same, in principle, as performing a compensating mean

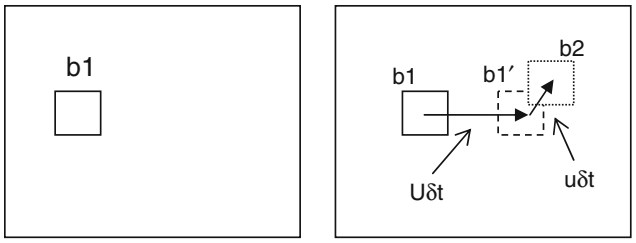

Fig. 2 **a** (*left*) and **b** (*right*) are sampled with a time interval, δt, between them. The correlation *box b1* in **a** is first moved by a pixel distance $U\delta t.s$, where s is a constant in units of pixels/cm. The new location of b1 is b1′, and it is from here that displacements are calculated by cross-correlation with candidate locations in a local neighbourhood. Here *box b2* is shown as the most likely displacement location in **b**. δt can now be expanded so that pixel distances $u\delta t.s$ are optimised

shift in cross-correlation box for the second image in a pair (the 2-camera system loses no pixels, and is significantly cheaper and more flexible). The principle is shown in Fig. 2. Adding a constant shift in one or more directions to remove a mean flow component in DPIV calculations is a standard option in most commercial codes, and it is a built-in component of the CIV algorithms used here. We now investigate the behaviour as δt is allowed to become very long, so that the compensating mean flow pixel displacements can be a significant fraction of the total number of pixels in the mean flow direction. Such a procedure can work, provided the light sheet is extremely carefully aligned with the mean flow, and provided the out-of-plane velocity component is small by comparison. These conditions can be met in a low-turbulence wind tunnel.

2.4 Analysis and notation

Estimates of the in-plane velocity components are made either through a fitting of a spline-fitted autocorrelation function to the computed cross-correlation function, or from a direct functional fitting of splined particle image windows. The displacement vector is located half way between the geometric centre of the initial image correlation window and its final estimated destination. The raw velocity field is interpolated back onto a regular rectangular grid through a smoothing thin-shell spline and gradient quantities are computed analytically from the spline coefficients themselves. Although errors in the velocity estimates are not constant fractions of the displacements, the most likely uncertainty in velocity estimates is not likely to exceed 1% and for the gradient quantities the figure is 5%. Fincham and Spedding 1997 and Fincham and Delerce (2000) may be consulted for further details. Note that although the CIV algorithms can be shown to be among the best available (e.g. Piirto et al. 2005), none of the results herein depend on details of the method. They all ultimately stem from the limited resolution at small scales that is common to all PIV methods.

The disturbance velocity, **u**, is described in terms of its components $\{u, v, w\}$ in directions $\{x, y, z\}$:

$$\left.\begin{aligned} u &= \tilde{u} - \bar{U} \\ v &= \tilde{v} \\ w &= \tilde{w} \end{aligned}\right\}, \tag{4}$$

where the tildes denote the original, measured quantities and $\bar{U}$ is the steady, time-averaged mean speed over the whole observation window, and over each image sequence. $\bar{U}$ is thus calculated from the prescribed integer pixel shift in the CIV calculation, plus the mean of any fractional part computed in CIV. Measurements are made over a vertical plane, aligned in the streamwise direction, with size $\Delta X \times \Delta Z$. The rms quantities for one single velocity field estimate are

$$\left.\begin{aligned} u' &= \sqrt{\frac{1}{mn}\sum_{i=1}^{m}\sum_{j=1}^{n} u^2(i,j)} \\ w' &= \sqrt{\frac{1}{mn}\sum_{i=1}^{m}\sum_{j=1}^{n} w^2(i,j)} \end{aligned}\right\}, \tag{5}$$

where the indices i, j cover the rectangular array of measurements in x and z, respectively. u' and w' are therefore spatial averages (also averaged over the effective exposure time, δt). The sampling rate for successive velocity field estimates is 10 Hz, dictated by the pulse-pair repetition rate of the laser. When time averages are made over a number of frames, they are denoted $\bar{u}(x,z)$ and $\bar{w}(x,z)$ for the spatial maps,

$$\left.\begin{aligned} \bar{u}(x,z) &= \frac{1}{N}\sum_{i=1}^{N} u_i(x,z) \\ \bar{w}(x,z) &= \frac{1}{N}\sum_{i=1}^{N} w_i(x,z) \end{aligned}\right\}, \tag{6}$$

where the u and w components are averaged locally at each grid location over a time series of length N so $\bar{u}$ and $\bar{w}$ are the temporal deviations from $\bar{U}$ at each interrogation point. If the fluctuations in u and w are normally distributed about a stationary $\bar{U}$ then as $N \to \infty$, $\overline{u'}, \overline{w'} \to 0$. It will also prove convenient to define spatially averaged values for $U(t)$ and $W(t)$ at each timestep:

$$\left.\begin{aligned} U(t) &= \frac{1}{mn}\sum_{i=1}^{m}\sum_{j=1}^{n} u(i,j) \\ W(t) &= \frac{1}{mn}\sum_{i=1}^{m}\sum_{j=1}^{n} w(i,j) \end{aligned}\right\}. \tag{7}$$

In all experiments reported here, the wind tunnel speed was set at a nominal value of 9.37 m/s, which is close to the cruising speed of the small birds studied in the Lund wind tunnel.

3 Results

3.1 Correction of lens distortion effects

In choosing large δt values, measurement of u' and w' become possible, but so do measurement errors of certain kinds. In particular, the particle images now move from one part of the camera lens to a significantly distant part, and the difference in lens distortion characteristics increases in significance with increasing δt. This can be seen in Fig. 3, which shows contours of measured $\bar{u}$ and $\bar{w}$, averaged over 10 velocity fields captured during 1 s. The contour patterns are coherent, and have magnitudes that exceed the likely value of the turbulence levels. They are characteristic of displacement across a pincushion pattern

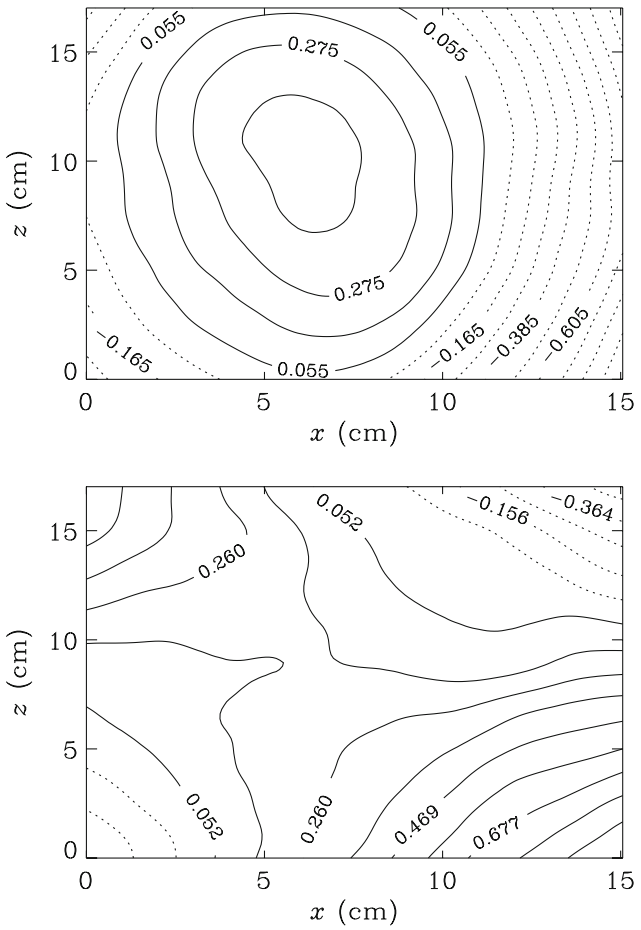

Fig. 3 Contours of time-averaged $\bar{u}$ (*top*) and $\bar{w}$ (*bottom*). Contour values are given in $\%U$. The DPIV exposure time, $\delta t = 2{,}000$ μs

lens distortion, and have the same shape as those found by Spedding et al. (2003a) and subsequently used as correction surfaces. The magnitude of these distortion patterns depends on δt, and here $\delta t = 2{,}000$ μs, a comparatively large value used to illustrate the phenomenon. However, anticipating use of such large values in these experiments, it is clearly necessary to compensate for this systematic error. Thus, for each δt, we define a mean residual field, calculated from the time-average of all frames in the data set (from 10 to 100),

$$\{u_r, w_r\} = \{\overline{u}, \overline{w}\}, \tag{8}$$

and then the best estimate of the fluctuating velocities is

$$\left.\begin{aligned} u &= \tilde{u} - \overline{U} - u_r \\ w &= \tilde{w} - w_r \end{aligned}\right\}. \tag{9}$$

A typical point-by-point convergence rate for the residual field is 0.72 after 10 timesteps, 0.85 after 20 steps and 0.96 after 50 steps. The mean residual field can be fitted by various order polynomial and spline surfaces, and these smoother functions can be used as a better estimate of the likely true residual field, but doing so has no effect on the measured statistics and we prefer to retain the computed mean field as the most direct approach.

3.2 Long DPIV exposures for turbulence measurement

The effect of varying δt on measured turbulence intensities is shown in Fig. 4. The apparent turbulence intensity magnitude is a strong function of δt. If the measurement were actually of turbulence, then its magnitude would be independent of δt. Instead, the result is an artefact of the finite resolution in measuring small displacements. Since

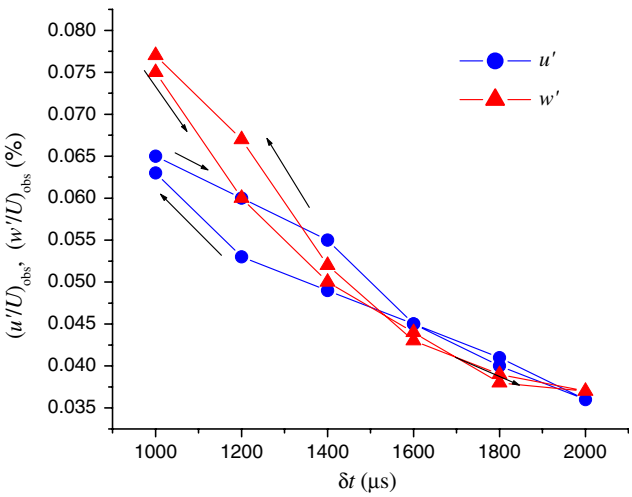

Fig. 4 Observed turbulence intensity in streamwise (u', *circles*) and vertical components (w', *triangles*), as a function of DPIV exposure time, δt. Each case is composed of a sequence of experiments with increasing δt (*arrows left to right*) and then decreasing δt

this algorithm error (which is usually dominated by some form of peak-locking error—see for example Fincham and Spedding 1997; Westerweel 1997; Prasad et al. 1992) is fixed in pixels (we may call it e_a), then as δt increases, so does the particle image displacement D, and so the relative error e_a/D decreases. The spurious dependence of q/U on δt can be used as a diagnostic of whether a DPIV method can be said to be measuring the flow physics or primarily discretisation errors.

The measurements show signs of convergence towards the lower right corner of Fig. 4, and that value of 0.035% is the same as previous hot-wire measurements in this wind tunnel (Pennycuick et al. 1997). Note that δt values are much larger than normally used during an experiment, where typically $80 \leq \delta t \leq 200$ μs. Figure 4 also shows that the results are independent of the elapsed time during the experiment and there is no hysteresis between the increasing and decreasing δt parts. Although Fig. 4 shows results that are related somehow to disturbance levels in the fluid, it is not clear that the values at the longest value of $\delta t = 2{,}000$ μs (on the right side of Fig. 4) are not still significantly affected by measurement error.

Figure 5 reports the results of an experiment using extremely long exposure times. Measured values of u'/U and w'/U continue to decrease as δt rises to 4,000 μs, but after $\delta t = 2{,}500$ μs, u'/U stabilises briefly and then fluctuates with increasing amplitude with further increases in δt. Beyond this point u'/U and w'/U behave differently. While u'/U varies around a mean value of 0.035%—its last reliably measured value—w'/U stabilises between 0.02 and 0.025%. The reasons for this behaviour will be discussed shortly, but for the moment, we note that, thus far, the best

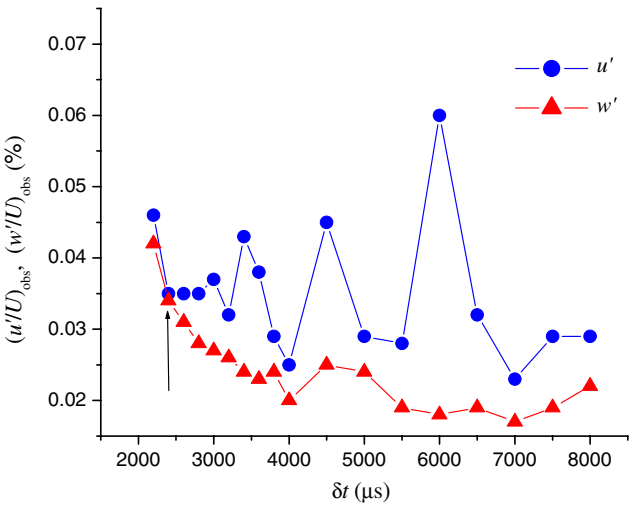

Fig. 5 Observed turbulence intensities (streamwise component, u' in *circles*, vertical component, w' in *triangles*) as function of long δt. At the *arrow*, the average u' measure stabilises, but with large amplitude fluctuations about that value

estimate of the turbulence level for this tunnel, if indeed it must be reduced to a single number, is approximately $q/U = \left((u'/U)^2 + 2(w'/U)^2\right)^{1/2} = 0.046\%$, where we assume that fluctuations normal to the mean flow have the same magnitude ($v' \approx w'$).

3.3 The structure of wind tunnel turbulence

If we are now measuring mostly true velocity fluctuations, and not measurement noise, then the disturbance velocity fields, estimated over some window of $\{x, z\}$ (which shrinks with increasing δt) contain information about the spatial structure. This structure (and the associated turbulence measurement itself) will reflect the true variations provided it is correct to imagine that it has convected along with the flow over a time δt and streamwise distance $U\delta t$. Figure 6 shows the spanwise or cross-stream vorticity,

$$\omega_y = \frac{\partial w}{\partial x} - \frac{\partial u}{\partial z},$$

and the divergence in the plane of measurement,

$$\Delta_y = \frac{\partial u}{\partial x} + \frac{\partial w}{\partial z}.$$

The two quantities have approximately equal magnitude, and show no preferred orientation.

Figure 7 shows the spectral distribution of kinetic energy over the range that can be resolved by the DPIV experiment. The energy is summed over circular shells of constant magnitude wavenumber $|k| = \left(k_x^2 + k_z^2\right)^{1/2}$. The result shown is an average over 100 velocity fields taken over 10 s. Most energy is at moderate length scales, from $1 \leq |k| \leq 4.5$, and at higher wavenumbers the kinetic energy has dropped an order of magnitude from its peak value. $k = 4.5$ rad/s corresponds to a length scale of about 1.5 cm. The magnitude and distribution of energy in the fluctuating velocity components is equal in the streamwise and vertical direction. The fluctuations at higher wavenumbers for $|k| > 8$ rad/s (or wavelengths <0.8 cm, which is four times the grid spacing) are almost certainly affected by the finite resolution of the CIV algorithm.

In this paper, the instantaneous spatial fluctuations in the otherwise uniform wind-tunnel flow are averaged for measurements of u' and w'. Hot-wire data construct the same measure from temporal fluctuations at a single point and the two methods are equivalent if the standard Taylor-hypothesis is invoked. Temporal fluctuations over time scales on the order of seconds can be measured from long sequences of DPIV images, and one such sequence is shown in Fig. 8. This figure shows that excursions of the mean streamwise velocity, $U(t)$ (defined in Eq. 7), of the order of 1 cm/s, or about 0.1% of the mean, can be reached

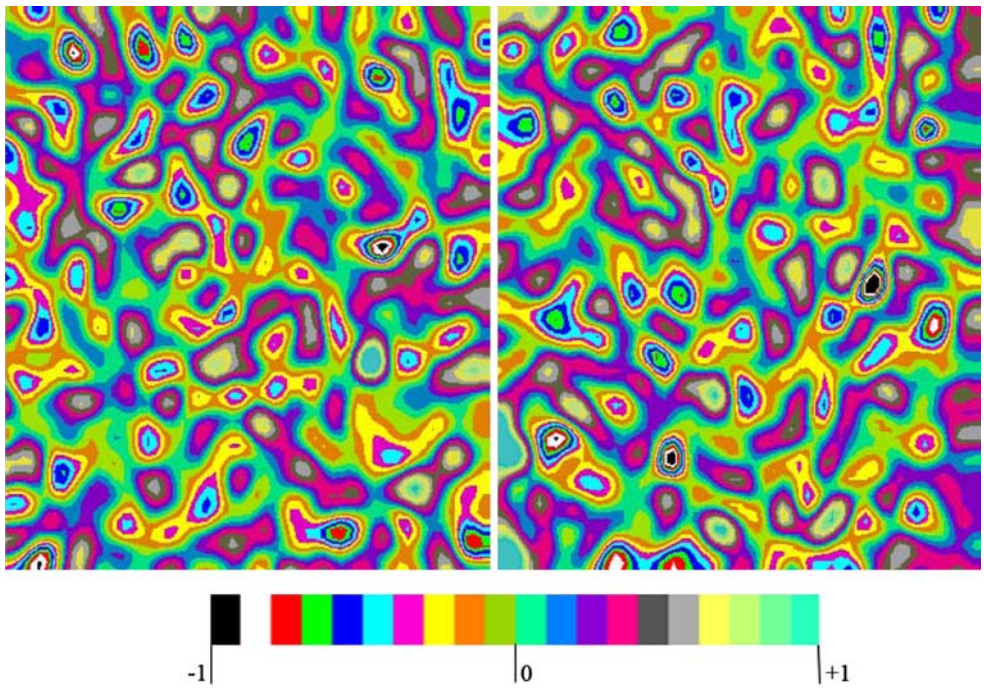

Fig. 6 Spanwise vorticity (*left*) and divergence in the plane of measurement (*right*). The field of view $\{\Delta X, \Delta Y\} = 14.5 \times 17$ cm. $\Delta X < \Delta Y$ because the x-range is reduced by the 131 pixel shift required to remove the mean flow for $\delta t = 2{,}400$ μs. The 20-step *colour bar* is mapped to ±1/s for both fields

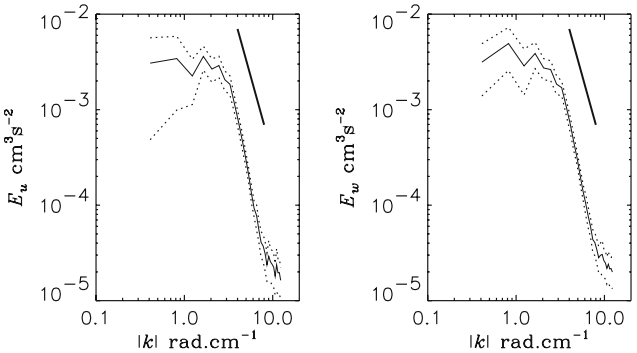

Fig. 7 Time-averaged energy spectra of the streamwise (*left*) and vertical (*right*) velocity fluctuations. The time-averaged spectra over 100 realisations are shown by the *solid lines* and banded by *dashed lines* at $\pm 1\sigma$ for each |k|. The *thick straight lines* have $|k|^{-5/3}$ slope

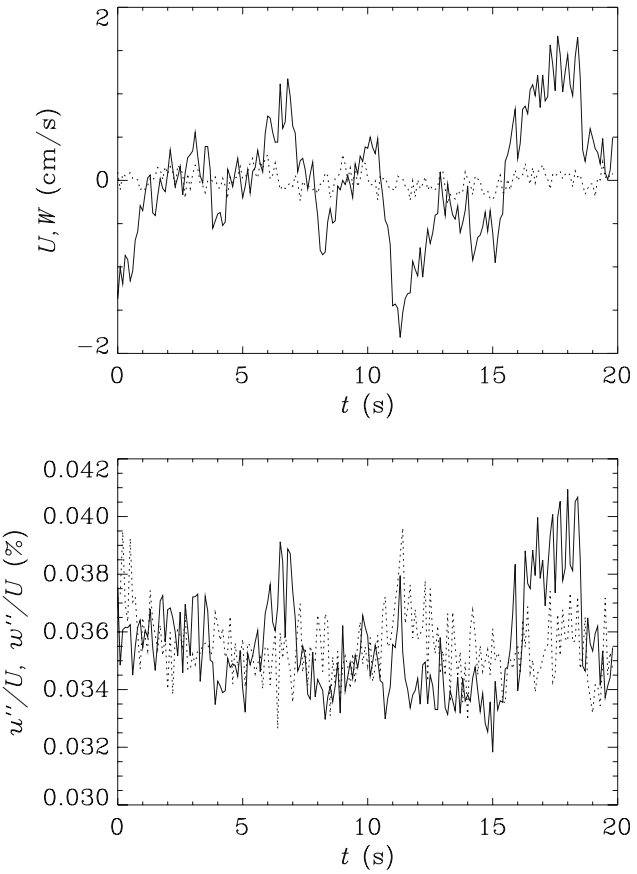

Fig. 8 *Above*: mean streamwise disturbance velocity, $U(t)$ (*solid line*) and vertical disturbance velocity, $W(t)$ (*dashed line*) from spatial averages at each timestep. *Below*: the corrected, fluctuating wind tunnel turbulence levels (u''/U is *solid line*, w''/U is *dashed*). The data come from one sequence of 200 images, with $\delta t = 2{,}500$ μs

in occasional bursts that have a timescale of between 3 and 4 s (the tunnel circulation time, $T_C \approx 30$ s). There are no corresponding fluctuations in the mean vertical velocity, W.

These variations in mean streamwise velocity could originate from the tunnel fan speed controller, or they could be due to variations in boundary layer thickness on the tunnel walls. The 0.1% corrections are small by most standards, but they can give a significant non-zero mean component to the instantaneous velocity fields if they are calculated from a mean over the whole time sequence. Indeed, this explains the increased and erratic fluctuations in u'/U for large δt in Fig. 5. The peak values are caused by regions where the entire window has some small mean value away from the global mean. We return to the

question of whether such motions should be counted in overall turbulence measures in the next section.

At each timestep, the local mean $U(t)$ and $W(t)$ (Eq. 7) may be removed from the $\{u, w\}(x, z)$ fields (Eq. 9),

$$\left.\begin{aligned} u''(t) &= \sqrt{\frac{1}{mn}\sum_{i=1}^{m}\sum_{j=1}^{n}(u(i,j)-U(t))^2} \\ w''(t) &= \sqrt{\frac{1}{mn}\sum_{i=1}^{m}\sum_{j=1}^{n}(w(i,j)-W(t))^2} \end{aligned}\right\}, \tag{10}$$

so that only spatial variation in the observation window contributes to the total. The lower part of Fig. 8 shows corrected time traces of u''/U and w''/U over the same time interval. Both measures vary around a mean value of about 0.036%. u''/U is weakly correlated with $|U|$, but it is not clear whether this variation is an artefact of the data reduction. Accelerations in U, for example, could be responsible for increased magnitude of u'', but they would also contribute to an extra residual in the $u(x, z, t) - U(t)$ calculation.

If the same correction is applied to data in Fig. 5, the result is Fig. 9, where the smoothness of u'' and its agreement with w'' has improved significantly. However, once again, there is a point, at $\delta t \approx 4{,}000$ μs, where the curves of u''/U and w''/U begin to separate and the variation in the result increases. Now, the long disturbance displacements (after the mean has been subtracted) of the groups of image particles responsible for the measured $\{u'', w''\}$ convect those particles to slightly different parts of the lens distortion correction surface (Fig. 3). This effect is taken into account to leading order by applying the correction of an averagely displaced group of particles, but small departures from this mean, due to local velocity gradients and accelerations can give spurious structure to the pattern of $\{u'', w''\}$, and affect the mean values. These spurious values will have some structure similar to the lens distortion curves of Fig. 3, since they are caused by relative motion on this surface. It is an effect that will always be present, and it is amplified as δt increases. A careful inspection of $\Delta_z(x, z)$ in Fig. 6b shows that the divergence field has some small remnant of circular symmetry, and the measured values are a projection onto this symmetry.

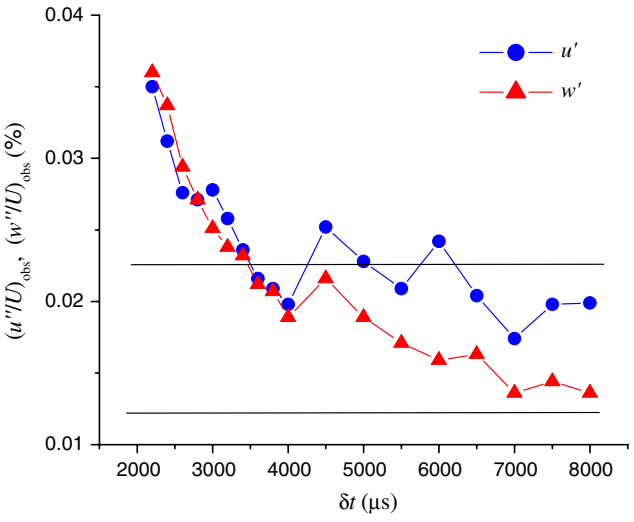

Fig. 9 Corrected turbulence intensities (streamwise component, u'' in *circles*, vertical component, w'' in *triangles*) from Fig. 5. Plausible values of the true turbulence level lie between the *horizontal bars*

The best estimates of u''/U and w''/U now appear to lie between 0.012 and 0.020%, which are significantly below the previous estimates derived from Fig. 5. If the fluctuations normal to U are again assumed to be isotropic, $q/U = 0.026\%$. Pennycuick et al. (1997) reported mean turbulence values of 0.035% (ranging from 0.031 to 0.037) over the same region of the same wind tunnel. Our lower estimate which compensates for momentary accelerations in the global flow, $U(t)$, is $q/U = 0.026 \pm 0.006\%$, while the upper limit is $q/U = 0.046 \pm 0.006\%$. Since the hot-wire estimates can be affected by mechanical vibrations, Pennycuick et al. noted that their measurements should be regarded as upper bounds. This brings up a more general question of how wind tunnel turbulence measurements can be calculated and reported.

4 Discussion

4.1 The basic problem

Having worked through the examples in these experiments, we may summarise the basic measurement problem using convenient numbers that are similar to those used here.

Suppose the mean flow speed, $U = 10$ m/s and the tunnel turbulence levels are given as 0.05%. Then $u' = 0.5$ cm/s. A DPIV exposure time, $\delta t = 2{,}000$ μs, gives a displacement due to turbulent motions of $u'\delta t = 10^{-3}$ cm. If a $2{,}048^2$ pixel array covers a 20 × 20 cm observation window, the scaling factor, $s \approx 100$ pixel/cm. A displacement of 10^{-3} cm is thus equivalent to δpix = 0.1 pixel. If the minimum expected error in the estimated pixel displacement is 0.02 pixel, the required measurement is only five times above the noise. Alternatively, if we stipulate that the pixel displacements due to turbulent fluctuations must be ten times the smallest measurable displacement, $\delta(\text{pix})_{\min}$, then a criterion for successful wind tunnel turbulence measurement can be given as

$$10\delta(\text{pix})_{\min} \leq u'\delta t.s.$$

Given an expected turbulence level, u', the experimenter must select an appropriate combination of DPIV exposure

time, δt, and magnification, s, onto the pixel array. Neither parameter can be increased without limit because errors due to optical nonlinearities essentially multiply both terms.

The required δt values of 2,000–4,000 μs in the example above are at least one order of magnitude above typical DPIV settings for flow measurements in such circumstances (given the same assumptions on sensor geometry, optical magnification and mean flow speeds), which cannot measure wind tunnel turbulence. The better the flow quality in the wind tunnel, the more acute the problem. Wind tunnels with four times higher turbulent fluctuation magnitudes are not four times easier to measure because the higher turbulence levels increase the likelihood of particles leaving even a perfectly aligned light sheet during the large required δt.

4.2 Reporting turbulence levels

A wing (or wing pair) of 5 cm chord flying at 10 m/s has a flow transit time of 5 ms. Fluctuations in the mean flow with periods of the order of 2–4 s therefore occur over at least 400 transit times, and so might reasonably be regarded as slow variations in U with little dynamical significance. Arguing thus, an appropriate estimate of the wind tunnel turbulence levels is 0.026%. On the other hand, if the control manoeuvres required by a gliding bird over the course of 10 s are being studied, then the higher value of 0.046%, which includes these longer-timescale variations, is more correct. In reporting rms turbulence values from hot-wire data, the mean value is always removed from the measured signal. In various statistical detrending operations, other long time period/low frequency components might be removed also, and removing the linear part of any global curve fit is also common, for example. The complete reporting of a wind tunnel turbulence level should therefore specify the effective range of time scales or frequencies over which it has been calculated.

4.3 Turbulence estimates from DPIV

The instantaneous structure of the fluctuating vorticity and divergence fields is shown in Fig. 6 for this wind tunnel, operating at one speed. The wavenumber range of energetic scales is given in Fig. 7. Together, they show that the fluctuating velocity field has no significant coherent large scale structure that is observable over this range of scales, and that most turbulence energy is contained within a wavenumber range of 1.5–6 rad/cm (the corresponding wavelengths are 1–4.2 cm). The frame size $\Delta X = 14.5$ cm and the grid spacing is 0.25 cm so the range of measurable wavenumbers in these figures is 0.43–12.5 rad/cm.

The Taylor hypothesis is routinely invoked by those making time-resolved turbulence measurements at a single point, and if convected along by the mean flow past a fixed measurement point (such as a hot wire), the frozen flow of Fig. 6 would appear as frequencies

$$f = kU/2\pi \in [64\,\text{Hz}\text{--}1.86\,\text{kHz}]. \tag{11}$$

The most energetic wavenumbers of $1.5 \leq |k| \leq 6$ rad/cm lie between 220 and 890 Hz. In order to obtain these data, DPIV exposure times, δt, of up to 4,000 μs were used. Based on this effective exposure time alone, the Nyquist frequency representing the highest accessible frequency, $f_{\text{Ny}} = 1/(2\delta t) = 125$ Hz. Figures 5 and 9 suggest that the minimum usable $\delta t = 2{,}500$ μs, where f_{Ny} is still 200 Hz.

The f_{Ny} determined by δt is in a reference frame moving with the mean flow, which is not the same as Eq. 11 above. Whether it is sufficient to resolve dynamically important time- and space-scales in the flow depends on the $\omega(k)$ relation for that flow. The basic point is that the larger the value of δt, the lower the upper limit of resolvable frequencies, and so δt cannot be increased without limit. Note that while the upper limit in observable frequencies affects the correct interpretation of the flow structure (in Fig. 6) and spectral distribution (Fig. 7), it does not necessarily affect the global (single number) statistics, as aliased frequencies still appear in the measured signal without loss of energy.

The estimated values of $q/U = 0.026$ and $0.046 \pm 0.006\%$, with and without low frequency correction, are consistent with those previously measured in hot wire experiments in the same wind tunnel, so the DPIV methods for measuring them appear to be reasonable.

4.4 Experiments in nominally low turbulence wind tunnels at transitional Reynolds number

Flows involving marginal stability of laminar boundary layers are very susceptible to ambient turbulence, and to small variations in model geometry and boundary conditions. Such is the case for tests on small-scale flying devices which may be human-engineered micro air-vehicles or naturally evolved birds or bats. Even though neither device normally flies through perfectly still air (if there were such a thing), generalisable and repeatable test results require that the background turbulence levels be low and also that the turbulence characteristics be well-documented. In addition to global averages, the spatial and temporal structure of the fluctuations should be characterised. This paper shows that DPIV methods can be used to measure the tunnel properties, given suitable operating conditions and particularly careful tuning of the DPIV parameters. If adequate wind tunnel turbulence properties are measured this way, they may yet be significantly

different when the test and/or diffuser section contains mounting struts, camera cables, mirrors or other common clutter, and should be measured again (Selig and McGranahan (2004), for example, show turbulence levels and spectra, together with spatial variation of the mean flow with the tunnel empty and with measurement apparatus installed).

Finally, we briefly note an application of the long-exposure DPIV method to detect a significantly non-uniform background flow that would not otherwise be measured. Otherwise uniform, low-turbulence background conditions can be significantly disrupted in practical animal flight experiments, when various markers and platforms or perches for regulation of flight are placed inside the wind tunnel. In some instances, safety nets are installed not only in the downstream diffuser section (a necessity!), but also in the front of the test section. These are often claimed to have little noticeable effect on flight performance, but now that a sufficiently sensitive measurement technique has been developed, the effect on the flow can be seen directly.

Figure 10 shows the disturbance velocity field caused by the upstream net superimposed on colour-coded cross-stream vorticity contours. There is a regular array of easily detectable, horizontal, laminar wakes, separated by opposite signed vorticity layers. The instantaneous wake structures (Fig. 10a) themselves show some signs of semi-regular variation in the streamwise direction. The time-averaged vorticity field (Fig. 10b) is taken from 20 independent timesteps and shows exactly the same regular variation in the vertical direction, but the horizontal variance is significantly reduced. The background turbulence cannot be seen on this scale because it is many times (about 30) smaller in magnitude. Small lens distortion effects can be seen at the grid edges, particularly at the bottom of the images as they could not be removed using the usual averaging methods employed for the tunnel turbulence estimates.

The net itself is composed of a 27 mm square mesh of threads with thread diameter 15.1 ± 0.4 μm. The Reynolds number based on thread diameter, d, $Re_d = 7$ for $U = 7$ m/s. The mean vertical spacing between wakes in Fig. 10b is 27.1 ± 0.03 mm, which is equal to the mesh spacing. Measurements were taken approximately 1 m downstream of the start of the test section, where the mesh was strung, and so $x/d \approx 66{,}000$. The low Reynolds number and comparatively low background turbulence levels lead to a perfectly preserved wake image of the mesh, far downstream of its origin. Pennycuick et al. (1997) previously documented an increase in global turbulence levels in the test section due to an upstream (but different) net. Here we see that a net actually imposes a rather stable, laminar pattern on the flow, which may or may not be aerodynamically important, but its presence ought to be noted, particularly in view of the sensitivity of wing performance to small disturbances.

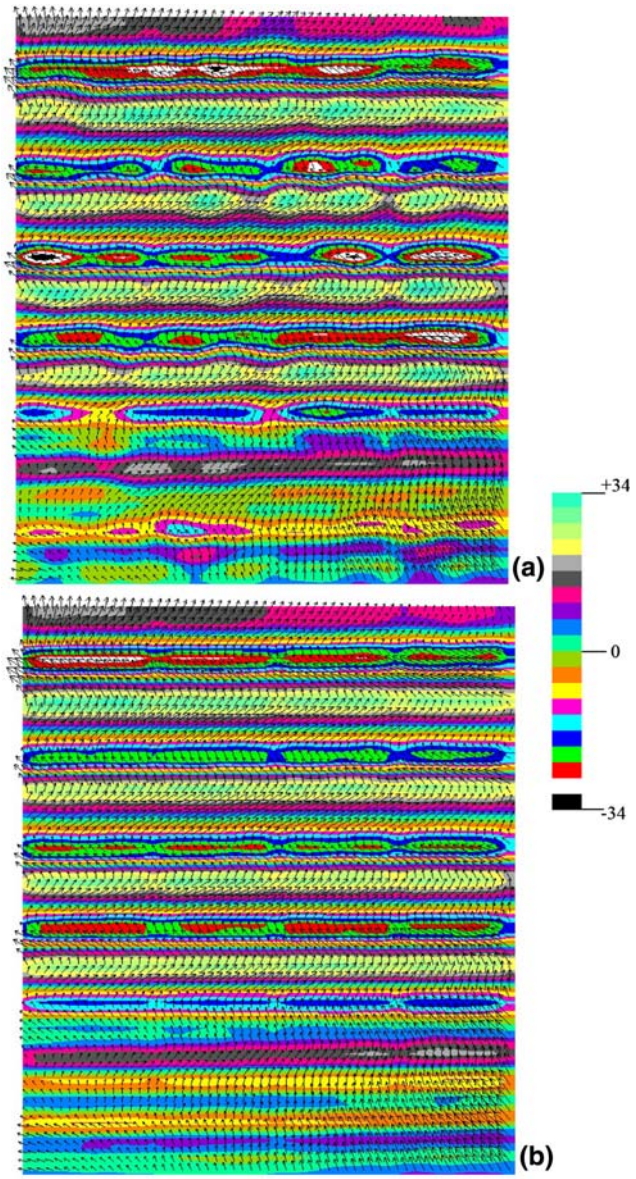

Fig. 10 Instantaneous (**a**) and time-averaged (**b**) spanwise vorticity, $\omega_y(x, z)$, for empty test section with upstream net. The field of view $\{\Delta X, \Delta Y\} = 14.5 \times 17$ cm, $\delta t = 2{,}500$ μs and vector displacements are shown 16 times their original length. $Re_d = 7$, based on net thread diameter

5 Summary

A single example case is described to demonstrate that, provided measurements are made with care and precision, the low turbulence levels in high quality low-speed wind tunnels can be estimated with DPIV methods. The fluctuation magnitudes are consistent with independent hot-wire

estimates, and the spatial patterns of the disturbance quantities in the measurement plane can also be found. The window of usable operating parameters is constrained by the requirement for large δt's on one hand, and higher-order corrections as disturbance quantities occupy different locations in the lens distortion correction surface on the other. Given perfect lighting and particle seeding, further improvements will benefit both from better optics and further advances in DPIV algorithms. A DPIV system that is correctly tuned to measure very small disturbance quantities is a valuable indicator of actual operating conditions, and the correct specifications of these (including the range of scales and frequencies over which global statistics are computed) will be particularly important in future experiments on the aerodynamics of birds, planes, bats and gliders at moderate Reynolds number.

References

Adeyinka OB, Naterer GF (2007) Measured turbulent entropy production with large eddy particle image velocimetry. Exp Fluids 42:881–891

Adrian RJ, Christensen KT, Liu Z-C (2000) Analysis and interpretation of instantaneous turbulent velocity fields. Exp Fluids 29:275–290

Agrawal A (2005) Measurement of spectrum with particle image velocimetry. Exp Fluids 39:836–840

Barlow JB, Rae WH, Pope A (1999) Low-speed wind tunnel testing. Wiley, New York

Dryden HL, Kuethe AM (1929) Effect of turbulence in wind tunnel measurements. NACA Report# 342

Dryden HL, Schubauer GB, Mack WC, Skramstad HK (1937) Measurements of intensity and scale of wind tunnel turbulence and their relation to the critical Reynolds number of spheres. NACA Report# 581

Fincham AM, Spedding GR (1997) Low-cost, high resolution DPIV for measurement of turbulent fluid flow. Exp Fluids 23:449–462

Fincham AM, Delerce G (2000) Advanced optimization of correlation imaging velocimetry algorithms. Exp Fluids 29:S13–S22

Hedenström A, Rosén M, Spedding GR (2006) Vortex wakes generated by robins *Erithacus rubecula* during free flight in a wind tunnel. J R Soc Interface 3:263–276

Hedenström A, Spedding GR (2008) Beyond robins: aerodynamic analyses of animal flight. J R Soc Interface 5:595–601

Henningsson P, Spedding GR, Hedenström A (2008) Vortex wake and flight kinematics of a swift in cruising flight in a wind tunnel. J Exp Biol 211:717–730

Hinds WC (1999) Aerosol technology: properties, behavior and measurement of airborne particles. Wiley, New York

Lavoie P, Avallone G, De Gregorio F, Romano GP, Antonia RA (2007) Spatial resolution of PIV for the measurement of turbulence. Exp Fluids 43:39–51

Lissaman PBS (1983) Low Reynolds number airfoils. Ann Rev Fluid Mech 15:223–239

Lyon CA, Broeren AP, Giguere P, Gopalarathnam A, Selig MS (1998) Summary of low-speed airfoil data, vol 3. SoarTech, H.A. Stokely, Virginia Beach

Muijres FT, Johansson LC, Barfield R, Wolf M, Spedding GR, Hedenström A (2008) Leading-edge vortices increase lift in bat flight. Science 319:1250–1253

Park KJ, Rosén M, Hedenström A (2001) Flight kinematics of the barn swallow (*Hirundo rustica*) over a wide range of speeds in a wind tunnel. J Exp Biol 204:2741–2750

Pennycuick CJ, Alerstam T, Hedenström A (1997) A new low-turbulence wind tunnel for bird flight experiments at Lund University, Sweden. J Exp Biol 200:1441–1449

Pennycuick CJ, Hedenström A, Rosén M (2000) Horizontal flight of a swallow (*Hirundo rustica*) observed in a wind tunnel, with a new method for directly measuring mechanical power. J Exp Biol 203:1755–1765

Piirto M, Eloranta H, Saarenrinne P, Karvinen R (2005) A comparative study of five different PIV interrogation algorithms. Exp Fluids 39:571–588

Prasad AK, Adrian RJ, Landreth CC, Offutt PW (1992) Effect of resolution on the speed and accuracy of particle image velocimetry interrogation. Exp Fluids 13:105–116

Rosén M, Hedenström A (2001) Gliding flight in a jackdaw: a wind tunnel study. J Exp Biol 204:1153–1166

Scarano F (2003) Theory of non-isotropic spatial resolution in PIV. Exp Fluids 35:268–277

Selig MS, McGranahan BD (2004) Wind tunnel aerodynamic tests of six airfoils for use on small wind turbines. NREL Report SR-500-34515

Spedding GR, Hedenström A, Rosén M (2003a) Quantitative studies of the wakes of freely-flying birds in a low turbulence wind tunnel. Exp Fluids 34:291–303

Spedding GR, Rosén M, Hedenström A (2003b) A family of vortex wakes generated by a thrush nightingale in free flight over its entire range of flight speeds. J Exp Biol 206:2313–2344

Tanaka T, Eaton JK (2007) A correction method for measuring turbulence kinetic energy dissipation rate by PIV. Exp Fluids 42:893–902

Tennekes H, Lumley G (1972) A first course in turbulence. MIT Press, Cambridge

Westerweel J (1997) Fundamentals of digital particle image velocimetry. Meas Sci Tech 8:1379–1392